Optical and x-ray evidence of the "de Vries" Sm-*A**–Sm-*C** transition in a non-layer-shrinkage ferroelectric liquid crystal with very weak interlayer tilt correlation

Jan P. F. Lagerwall* and Frank Giesselmann†
Institute of Physical Chemistry, Clausthal University of Technology, D-38678 Clausthal-Zellerfeld, Germany

Marc D. Radcliffe
3M Company, St. Paul, Minnesota 55144

(Received 10 March 2002; published 11 September 2002)

A non-layer-shrinkage fluorinated ferroelectric liquid crystal compound, 8422[2F3], has been characterized by means of optical, x-ray, and calorimetric methods. The orientational distribution within macroscopic volumes, determined through wide-angle x-ray scattering and birefringence measurements, was found to be identical in the Sm-*A** and helical Sm-*C** phases. Together with the absence of layer shrinkage, this constitutes strong evidence that the second-order Sm-*A**–Sm-*C** transition in this material is well described by the diffuse cone model of de Vries. The absolute values of the layer spacing show that the molecules aggregate to antiparallel pairs. The molecular interaction across the layer boundaries will then occur only between fluorine atoms, leading to unusually weak interlayer tilt direction correlation. This explains the experimental observations of a very easily disturbed Sm-*C** helix and a peculiar surface-stabilized texture. Tilt angle and birefringence values as a function of field and temperature have been evaluated in the Sm-*A** and Sm-*C** phases and the results corroborate the conclusions from the x-ray investigations.

DOI: 10.1103/PhysRevE.66.031703 PACS number(s): 61.30.−v, 64.70.Md, 61.30.Eb, 77.84.Nh

I. INTRODUCTION

The molecular origin of the optical tilt observed in Sm-*C* liquid crystals has been an issue of debate ever since the discovery in the early 1970s that a compound exhibiting Sm-*A* and Sm-*C* phases generally has a temperature dependent tilt angle Θ [1]. In the last few years the question has received renewed interest due to the recognition of its importance in the manufacturing of high-quality electro-optic devices based on ferroelectric or antiferroelectric, i.e., chiral Sm-*C** or Sm-C_a^*, liquid crystals (FLCs, AFLCs). The main obstacle in the commercialization of such devices has turned out to be the problems related to the shrinking of the smectic layers which occurs at the transition from the orthogonal (director parallel to the layer normal) Sm-*A** phase to the tilted Sm-*C** (or Sm-C_a^*) phase. As the layers are positionally anchored at the surfaces, they will then buckle in a chevron geometry which is the only one compatible with the new combination of surface and bulk conditions [2]. Accompanying the development of the chevron structure is the formation of so-called ''zig-zag'' defects and a reduction in effective optical tilt angle, effects which seriously degrade the quality of any electro-optic device.

The exact connection between director tilting and layer thickness change is, however, still not fully understood, and different materials show varying degree of shrinkage as a result of the tilting transition. In fact, a number of FLC materials displaying virtually constant smectic layer spacings *d* have been identified [3–5], and these materials have therefore come to receive a substantial interest from industry as well as academia. An understanding of why such materials do not show a shrinkage of the layers at the Sm-*A**–Sm-*C** transition, and why others do, is not only a key issue for the development of FLC and AFLC electro-optic devices, but it is also extremely interesting from a fundamental research point of view.

A number of models have been proposed to explain the non-layer-shrinkage (in this paper abbreviated NLS) *A*-*C* transition, the three fundamental ideas of which are illustrated in Fig. 1. For explaining the common observation of a Sm-*A* layer spacing which is smaller than the length of the maximally elongated molecules, Diele *et al.* [6] suggested that the molecules exhibit a kinked conformation with their cores orthogonal but the end chains tilted in this phase. Bartolino *et al.* [7] instead proposed the kinked conformation for the Sm-*C* phase, now with end chains orthogonal and the cores tilted, assuming that the molecules are elongated and orthogonal in the Sm-*A* phase. Such a scheme cannot explain a constant layer spacing, but explains well the one which varies much less than would be expected from the magnitude of the optical tilt angle. Combining these two models, assuming fluctuating tilted end chains in both phases, but with decreasing magnitude in Sm-*C**, Buivydas *et al.* [8] constructed a constant *d*.

The next idea, Fig. 1(b), regards the packing of the molecules and the nature of the layer interfaces. If one allows for a relatively large degree of molecular interdigitation between adjacent layers in the Sm-*A* phase, but not in the Sm-*C* phase, a layer spacing not affected by the tilting of the molecules may result [9,10]. The last class of ideas, Fig. 1(c), was initially presented by de Vries [11–14] and Leadbetter [15]. The basis is simply the recognition that the nonperfect

*Also at Department of Microelectronics and Nanoscience, Chalmers University of Technology, SE-412 96 Gothenburg, Sweden.

†Electronic address: giesselmann@pc.tu-clausthal.de

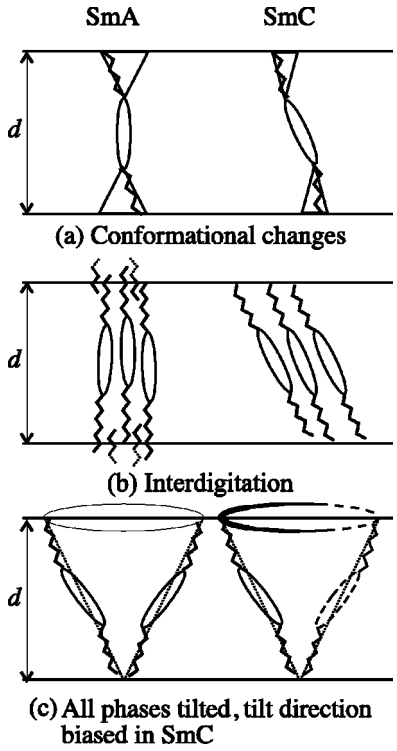

FIG. 1. The three different model schemes proposed for explaining smectic-*A*–smectic-*C* transitions without a decrease in layer spacing *d*. For explanations, see text.

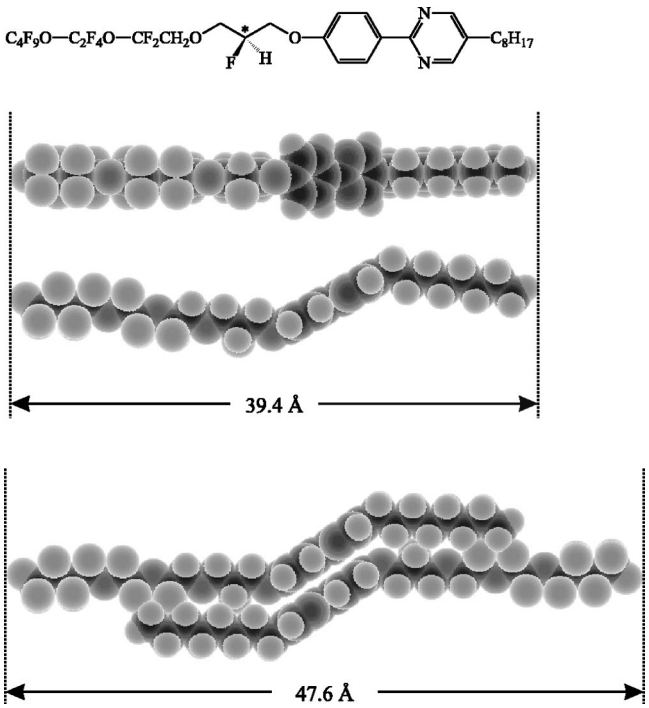

FIG. 2. Chemical constitution of the non-layer-shrinkage FLC 8422[2F3]. The length *l* of a single maximally extended molecule, as well as that of an aggregate consisting of two antiparallelly oriented molecules in this conformation, as suggested by Rieker and Janulis [19,20] for similar compounds, are also given.

orientational order present in all liquid crystals will lead to a nonzero mean square molecular tilt. The most probable orientation of the molecular long axis will not be along the layer normal, but on the surface of a cone centered around the layer normal, and de Vries therefore coined the term ''diffuse cone model'' for this description of smectic phases. The absence of a macroscopic optical tilt in Sm-*A* phase is explained by a uniform distribution of the tilt directions. The transition to a tilted phase can, in this model, occur simply through an ordering of tilt directions, a process which would not in itself produce any change in *d*.

In this paper we present detailed optical and x-ray measurements on an NLS ferroelectric liquid crystal exhibiting a large electroclinic effect in the Sm-*A** phase and analog, ''*V*-shaped,'' electro-optic response with very low saturation field (1 V/μm) in the Sm-*C** phase. We estimate the orientational distribution function in the Sm-*A** and helical Sm-*C** phases, and we thus show that this is probably the best example so far of materials exhibiting the de Vries diffuse cone model *A**-*C** transition. The de Vries model has received much attention lately (e.g., Refs. [3,4,16–18]), but it is sometimes described in a slightly different manner. In most modern reports, it is the Sm-*A** phase which is regarded as being unusual in de Vries type materials. We will, however, show that such a stance can be rather misleading, and that it is the de Vries Sm-*A**–Sm-*C** *transition* which should be regarded as truly unique in these compounds.

II. EXPERIMENT

The chemical constitution of the material, code named 8422[2F3], is given in Fig. 2. The phase sequence obtained by differential scanning calorimetry (DSC) and optical microscopy on planar-aligned samples is

$$\text{crystal} \underset{43.1\,^\circ\text{C}}{\leftrightarrow} \text{Sm } C^* \underset{64.5\,^\circ\text{C}}{\leftrightarrow} \text{Sm } A^* \underset{91.0\,^\circ\text{C}}{\leftrightarrow} \text{isotropic}.$$

For x-ray studies, the material was filled into Mark capillary glass tubes of 0.7 mm diameter and for optical microscopy studies we used commercial planar-aligning cells (E.H.C. Co. Ltd.) with a cell gap of 2 μm, or wedge-shaped cells (0.5–13 μm cell gap) described in detail in a previous paper [21]. The rubbed polyimide alignment layers in our cells had no influence over the direction of the layer normal as the Sm-*A** layers formed on cooling from the isotropic liquid. Nylon alignment layers have better effect, but were not available at the time of our experiments. In order to achieve reasonably uniform director orientation, a rather unconventional shearing technique was utilized. While cooling the sample past the *A**-*C** transition with an ac field applied, the vibrating shaft of an electric toothbrush was pressed onto the outer cell surface, inducing a shear-flow through which a uniform alignment could be obtained. For cell gaps below 3 μm, the result was good enough to allow electro-optic measurements in a microscope, using a 20× objective lens, a 2.5× photoocular lens, and a photodiode (FLC Electronics). All optical studies were carried out with the sample placed in an Instec MK1 hot stage fitted to an Olympus BH-2 polarizing microscope. The actual sample temperature was monitored with a PT100 sensor inserted into the sample holder.

For the x-ray measurements, a Cu-K_α radiation source was used. Small-angle scattering data from unaligned (powderlike) samples were obtained using a Kratky-compact camera (A. Paar) and a one-dimensional electronic detector (M. Braun), giving a measure of d with a resolution better than 0.1 Å in the range of interest. In order to measure the molecular orientational distribution, we also used an imaging plate system (Fuji BAS SR) for recording the two-dimensional scattering patterns from aligned samples. Scattering angles between $2\theta \approx 2°$ and $2\theta \approx 30°$ were covered. The fluorinated tails of 8422[2F3] unfortunately make it a poorly scattering compound in the wide-angle regime, and the diffraction images are therefore not as intuitively descriptive as for many other liquid crystals. Nevertheless, by evacuating the camera and prolonging the x-ray illumination, images good enough for quantitative analysis were obtained. The sample was mounted on a brass block, the temperature of which was regulated by a Eurotherm temperature controller, and kept in a 1 T magnetic field for alignment.

High-resolution measurements of the tilt angle Θ and birefringence Δn were performed using a temperature scanning technique, described in detail by Saipa and Giesselmann [22]. In brief, the method is based on monitoring of the sample temperature and optical transmission with close time intervals and high resolution, while slowly heating or cooling the sample throughout the mesophases at a constant rate. The scan was repeated in four different measuring geometries: crossed and parallel polarizers, and, for each case, layer normal $\hat{z}$ parallel and at 45° angle to the polarizer direction $\hat{p}$. With these four data sets, the transmittances between crossed polarizers, when the sample is oriented with $\hat{z}$ parallel to $\hat{p}$, τ_1, or at 45° to $\hat{p}$, τ_2, can be calculated. As the optical tilt angle θ is a function of the quotient τ_1/τ_2, and the birefringence Δn a function of the sum $\tau_1+\tau_2$, these parameters can now be extracted. Since it was impossible to achieve a perfectly uniform and defect-free alignment, a slight light leakage was measured even in the field-free Sm-A^* phase when the average $\hat{z}$ was parallel to one of the polarizers. This transmission value, which theoretically should be zero, was therefore subtracted from all measurements. This method worked very well for tilt angles above $\sim 5°$ but for $\theta \approx 0$ the errors may have a larger effect, hence giving the values at the very onset of tilt some uncertainty. Data were collected in the relaxed state as well as during switching. In the latter case, a 55.1 Hz square wave, supplied by a Hewlett-Packard 8116A function generator connected to a Krohn-Hite 7500 amplifier, was applied to the sample. Textures were photographed using a Nikon Coolpix digital camera replacing the photodiode. A Perkin Elmer DSC 7 was used for calorimetric measurements, on cooling and on heating at 5 K/min.

III. RESULTS AND DISCUSSION

A. Thermodynamics of the non-layer-shrinkage Sm-A^*–Sm-C^* transition

Most of the early NLS materials showed an unusually high transition enthalpy at the Sm-A–Sm-C transition (e.g., Refs. [14,23]) and this led many to believe that the transition in such smectics was always of first order. Such a conclusion would fit well with the conformational change model [Fig. 1(a)] which can hardly be imagined compatible with a continuous phase transition. Later on, however, reports of materials with a second-order A-C transition without layer shrinkage appeared [3,4]. It is thus clear that one cannot make any direct connections between the order of the phase transition and the temperature dependence of d.

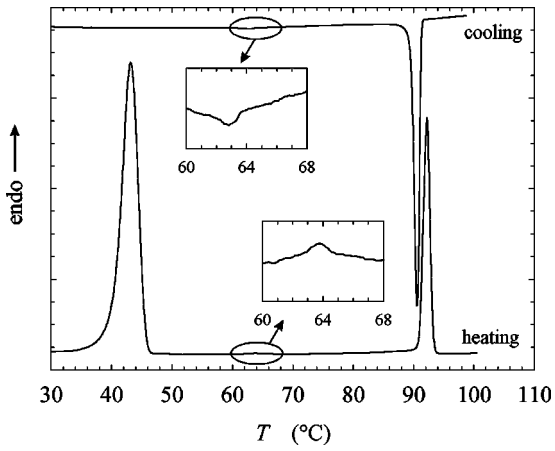

FIG. 3. DSC thermogram on heating and on cooling ($5\ \mathrm{K\,min^{-1}}$) of 8422[2F3]. The insets show magnifications of the region in which the second-order Sm-C^*–Sm-C^* transition takes place.

In Fig. 3, the DSC thermogram obtained for 8422[2F3] is shown. The very small λ-shaped singularity in the baseline, close to 64 °C, indicates a second-order A^*-C^* transition, which is confirmed by the optical measurements described in Sec. III C. The compound should thus in the first instance be compared with other second-order transition NLS materials. Among these, the compound studied by Radcliffe *et al.* [4], denoted 8/422, is an achiral smectic with a molecular structure very similar to that of 8422[2F3]. It turned out that the key element in producing the NLS properties of 8/422 is the fluoroether tail. The core structure could be modified without losing the desired properties. The compound is thus in this respect very different from the first-order transition NLS materials studied by Mochizuki *et al.* [23], where the naphthalene component of the core structure is the essential building block. The other known second-order NLS material, 9HL [3], is a nonfluorinated FLC belonging to a homologous series where the $d(T)$ behavior changes very much with end chain length, thus again indicating a large importance of the end chain geometry for the non-layer-shrinkage properties.

B. X-ray measurements

1. The smectic layer spacing

The layer spacing as a function of temperature, determined by small-angle x-ray scattering (SAXS) from a non-aligned sample, is given in Fig. 4. After a slight increase on cooling through the Sm-A^* phase, d decreased marginally after the transition to the Sm-C^* phase. The decrease was very small: the minimum value, observed 15 K below the transition, was only 0.3 Å less than the layer spacing mea-

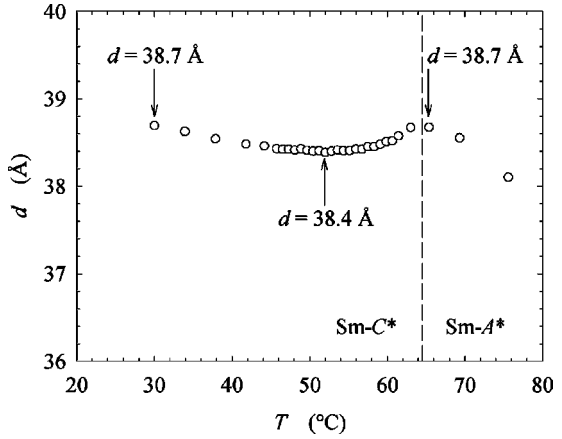

FIG. 4. Layer spacing d of 8422[2F3] as a function of temperature T, as obtained from small-angle x-ray scattering (SAXS) measurements on cooling through the Sm-A^* phase. Note that the variation within the Sm-C^* phase is only 0.3 Å.

sured at the Sm-A^*–Sm-C^* transition. On further cooling, d again increased and at room temperature the value had actually regained the value 38.7 Å observed at the onset of optical tilt.

Comparing with Fig. 2, we note that the layer spacing is only marginally smaller than the length l of the fully extended molecule ($l-d<1$ Å). The usual relationship is that the layer spacing, also in a Sm-A (A^*) phase, is considerably smaller than l [13]. We will have reason to return to this important observation in the following discussion of the orientational order.

2. The orientational distribution

An important aspect of de Vries' work, which is today often forgotten, was the recognition that the degree of orientational order has a significant impact on the layer spacing d actually observed in a smectic liquid crystal. Let us consider a smectic-A liquid crystal consisting of orientationally disordered rigid rods with length L. In this case d is given by the average

$$d = L\langle \cos\beta \rangle, \tag{1}$$

where β denotes the inclination angle between the rod and the smectic layer normal. The degree of inclination is usually measured by the (nematic) orientational order parameter,

$$S_2 = \frac{1}{2}(3\langle \cos^2\beta \rangle - 1). \tag{2}$$

Expanding Eq. (1) and Eq. (2) up to second-order terms in β,

$$d \approx L\left(1 - \frac{\langle \beta^2 \rangle}{2} + \cdots\right), \tag{3}$$

$$S_2 \approx 1 - \frac{3}{2}\langle \beta^2 \rangle + \cdots \tag{4}$$

and eliminating $\langle \beta^2 \rangle$ we obtain

$$d \approx \frac{L}{3}(S_2 + 2), \tag{5}$$

which in the limit $S_2 \to 1$ describes how d depends on the orientational order parameter S_2. Equation (5) clearly shows that d equals the rod length L in the case of perfect orientational order, $S_2 = 1$, only. In any case of orientational disorder ($S_2 < 1$) the smectic layer spacing is reduced in comparison to L. Since typical values of the orientational order parameter in Sm-A liquid crystals are within $S_2 = 0.7$–0.8, we have to expect d values that are 7–10 % lower than L and, in fact, this reduction is actually observed for most Sm-A materials.

According to Eq. (4), a Sm-A order parameter of $S_2 = 0.8$ corresponds to a root mean square inclination of $\sqrt{\langle \beta^2 \rangle} = 21°$ which clearly demonstrates that, even in a regular Sm-A phase, the rodlike molecules are substantially inclined with respect to the layer normal $\hat{z}$. But as the rods incline randomly towards all possible directions, the average inclination is zero and the director $\hat{n}$ is found to be parallel to $\hat{z}$.

At the transition to the Sm-C phase, the directions of inclination, φ, become ordered, giving rise to a nonzero tilt angle θ between the $\hat{n}$ and $\hat{z}$. As recognized by de Vries, this ordering in itself does not affect $\langle \cos\beta \rangle$ and thus the smectic layer spacing d remains constant if the transition is completely described by this ordering process. In contrast to such a ''de Vries type'' of transition, regular A–C transitions are in addition connected to a further increase of average molecular inclination, reducing $\langle \cos\beta \rangle$ and, thereby, the smectic layer spacing d. The de Vries type transition, which is probably best regarded as a limiting case in a spectrum of A–C transition types, can thus easily be recognized by tracking the evolution of the orientational distribution function (ODF) $f(\beta)$ while cooling from SmA to SmC. If this remains unaffected by the transition, the average molecular inclination is constant and the transition must follow the de Vries scenario.

We investigated $f(\beta)$ in the Sm-A^* and Sm-C^* phases of 8422[2F3] by wide-angle x-ray scattering (WAXS) experiments on samples uniaxially aligned in a moderate magnetic field (~1 T). Selected examples of the diffraction patterns are shown in Fig. 5. At small scattering angles, close to the beam stop, the diffraction pattern of the aligned Sm-A^* phase (left image, upper row in Fig. 5) shows sharp first- and second-order (pseudo-) Bragg peaks along the meridian, i.e., along the direction of the aligning field (horizontal, $q_\parallel$ in Fig. 5). These peaks, which reflect the quasi-long-range positional smectic order, clearly show that the layers are well aligned with their normals along the magnetic field.

At larger angles, corresponding to the periods of 4–5 Å typical of the transverse intermolecular spacing, a diffuse scattering originating from the liquidlike intralayer correlation is seen. Its intensity exhibits a directional modulation reflecting the orientational order of the rodlike molecules in the scattering volume with respect to the magnetic field direction. Since the direction of the smectic layer normal $\hat{z}$

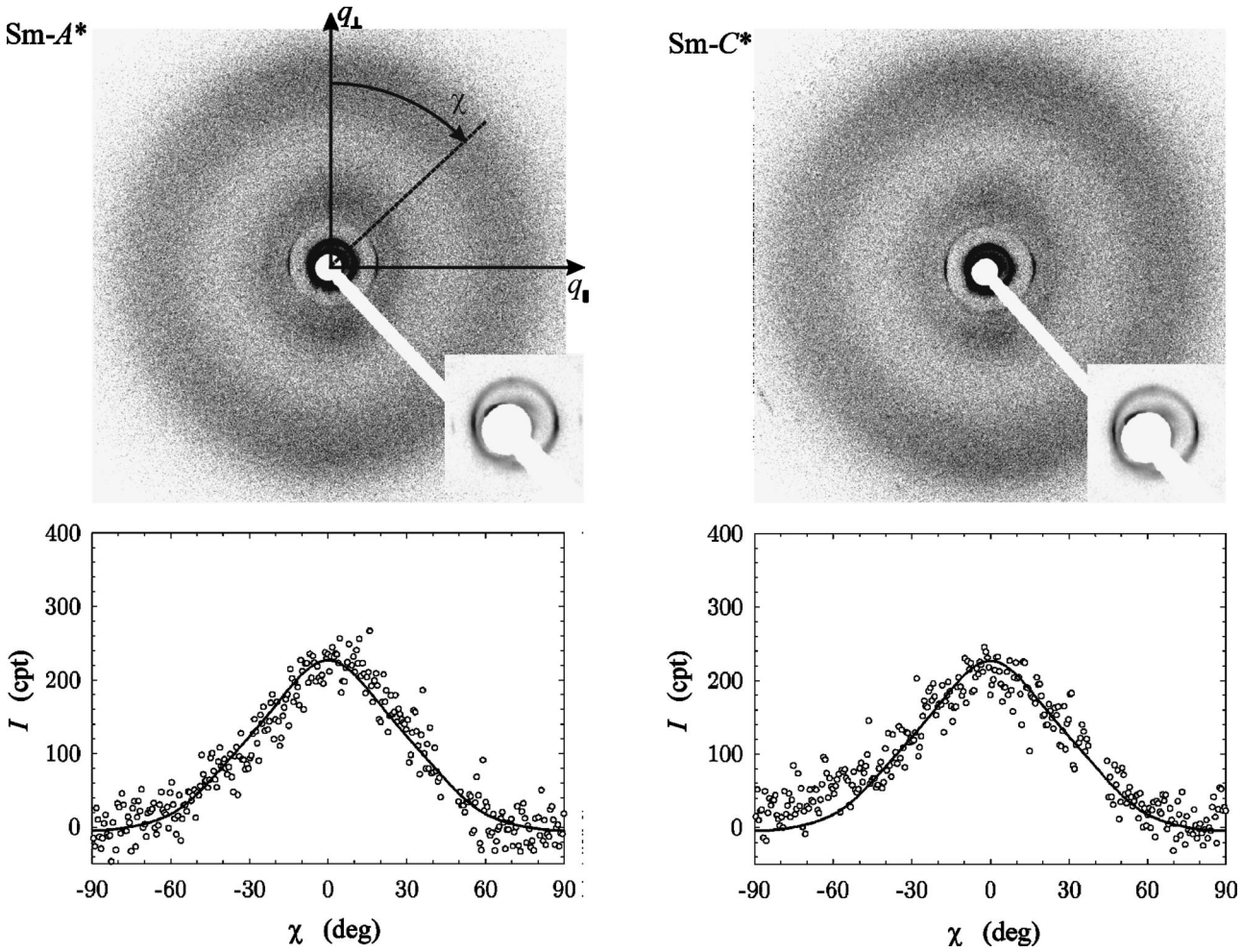

FIG. 5. Upper row, x-ray diffraction patterns in the Sm-A^* (left) and Sm-C^* (right) phases of 8422[2F3]. The magnetic field is oriented horizontally (meridional direction). Since the scattering intensities in the small- and wide-angle regimes are very different, the layer spacing peaks are reproduced with lower contrast in the insets. Lower row, the directional scattering profile $I(\chi)$, as obtained by radial integration over the wide-angle regime in the diffraction patterns. The continuous curves are best fits of Eq. (8) to the experimental data obtained in the Sm-A^* phase.

coincides with the field direction, the intensity profile $I(\chi)$ (cf. Fig. 5) directly probes $f(\beta)$, the orientational distribution function of the rodlike molecules with respect to the layer normal $\hat{z}$.

As expected, $I(\chi)$ measured in the Sm-A^* phase exhibited a maximum on the equator ($q_\perp$, cf. Fig. 5). Much more surprising was the observation that the diffraction pattern did not change at all by cooling the sample into the Sm-C^* phase (right image, upper row in Fig. 5). In sharp contrast to what is usually observed at smectic A-C and A^*-C^* transitions, neither a splitting of the layer reflection (indicating a tilt of $\hat{z}$ with the $\hat{n}$ fixed in the magnetic field direction) nor a broadening along χ of the diffuse wide-angle maximum (indicating a tilt of $\hat{n}$ with $\hat{z}$ fixed in the magnetic field direction) was observed. The absence of change gives clear evidence that the total orientational distribution of the molecules in the scattering volume is not affected by the A^*-C^* transition. While this is very difficult to explain with a model where the molecules in the Sm-A^* phase are oriented parallel to the layer normal, such a scenario is actually just what is to be expected at a de Vries type transition from Sm-A^* phase to helical Sm-C^* phase. In Sm-A^* phase we have rodlike molecules tilted by a certain average angle $\langle\beta\rangle$, all possible tilt directions φ being equally probable. At a de Vries transition to Sm-C^* phase, $\langle\beta\rangle$ remains constant but the direction of tilt becomes ordered. As we have a chiral Sm-C^* phase, the preferred direction of tilt spirals helically along the direction of the smectic layer normal. During the Sm-C^* experiments, we observed a brightly colored selective reflection from the sample, indicating the formation of the helical Sm-C^* superstructure. The selective reflection from homeotropically aligned 8422[2F3] has been measured at 404 nm wavelength, which roughly corresponds to a helical pitch of 270 nm (assuming an average index of refraction of 1.486). Integrated over a full pitch length, we therefore observe, like in SmA^*, all possible values of φ with the same probability. As long as $f(\beta)$ remains unchanged, and the helical pitch is smaller than the dimensions of the scattering volume, the two configurations, SmA^* and helical SmC^*, cannot be distinguished by the x-ray experiment and thus produce identical diffraction patterns.

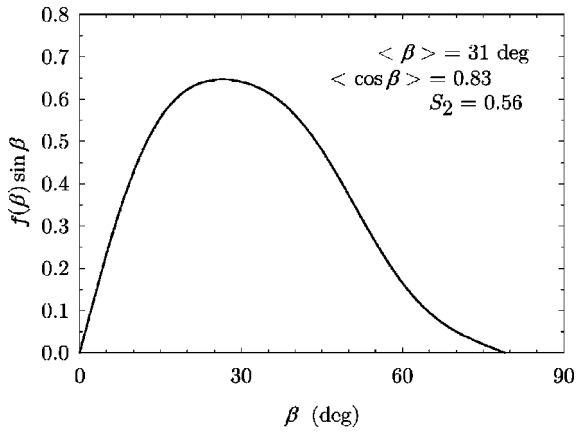

FIG. 6. The function $f(\beta)\sin\beta$ as obtained by fitting Eq. (8) to the experimental wide-angle scattering data, $I(\chi)$. The average molecular inclination $\langle\beta\rangle$, the average projection factor $\langle\cos\beta\rangle$, and the orientational order parameter $S_2=\langle P_2(\cos\beta)\rangle$, calculated from $f(\beta)\sin\beta$, are given in the inset.

We investigated the orientational distribution function $f(\beta)$ by a numerical analysis of the scattering profile $I(\chi)$ obtained for the Sm-A^* phase (left diagram, lower row in Fig. 5). In their classic paper [15], Leadbetter *et al.* derived the following relation between $f(\beta)$ and $I(\chi)$:

$$I(\chi)=\int_{\beta=\chi}^{\pi/2}\frac{f(\beta)\sin\beta\sec^2\chi}{\sqrt{\tan^2\beta-\tan^2\chi}}d\beta. \tag{6}$$

This equation provides an easy means of calculating the intensity profile $I(\chi)$ resulting from a given orientational distribution $f(\beta)$, but in order to do the opposite, extract $f(\beta)$ from the experimentally determined $I(\chi)$, a difficult numerical inversion is needed. In 1995, Davidson, Petermann, and Levelut [24] presented a refined procedure that allowed a simpler and more direct evaluation of $f(\beta)$. Instead of expanding the ODF in a series of Legendre polynomials, the coefficients of which correspond to the orientational order parameters $S_2, S_4, \ldots$, they proposed an expansion in terms of $\cos^{2n}$ functions,

$$f(\beta)=\sum_{n=0}^{\infty} f_{2n}\cos^{2n}\beta. \tag{7}$$

They then showed that the resulting intensity profile derived from Eq. (7) is also described by a series of $\cos^{2n}$ functions involving the same f_{2n},

$$I(\chi)=\sum_{n=0}^{\infty} f_{2n}\frac{2^n n!}{(2n+1)!!}\cos^{2n}\chi. \tag{8}$$

Hence, by fitting Eq. (8) to the experimental scattering profile $I(\chi)$, with the f_{2n} being the parameters to fit, $f(\beta)$ can directly be calculated by inserting the fitted f_{2n} into the expansion in Eq. (7).

The best fit of Eq. (8) to the Sm-A^* data of 8422[2F3] is shown as a solid line in Fig. 5. The curve is actually drawn in both lower diagrams in order to clearly illustrate how well the orientational distribution function determined for the Sm-A^* phase describes also the Sm-C^* data. In Fig. 6 we have plotted, instead of the actual $f(\beta)$ calculated according to Eq. (7) with the fitted f_{2n}, the more instructive orientational *probability* distribution function $f(\beta)\sin\beta$, which directly gives the probability to find a rodlike molecule inclined by an angle between β and $\beta+d\beta$. As directly seen from the maximum in the curve, the most probable inclination angle of the molecules in the Sm-A^* and Sm-C^* phases of 8422[2F3] is fairly high, about 25°.

With the distribution function $f(\beta)\sin\beta$ in Fig. 6, we can (numerically) calculate any average or expectation value $\langle X\rangle$ of a certain property X related to the probability distribution $f(\beta)\sin\beta$,

$$\langle X\rangle=\frac{\int_{\beta=0}^{\pi/2} X f(\beta)\sin\beta d\beta}{\int_{\beta=0}^{\pi/2} f(\beta)\sin\beta d\beta}. \tag{9}$$

With $X=\beta$ we obtain the average inclination angle $\langle\beta\rangle=31°$ for the rodlike molecules in the Sm-A^* and Sm-C^* phases of 8422[2F3]. In comparison to the general estimations given at the beginning of this section, this value is quite high and points towards a substantial orientational disorder in the smectic phases of this compound. To confirm this observation, we also calculated the orientational order parameter S_2 by using Eq. (9) with $X=(3\cos^2\beta-1)/2$ and obtained $S_2=0.56$, a value 20–30 % lower than the typical $S_2=0.7$–0.8 in ordinary Sm-A and Sm-A^* phases.

With respect to the smectic layer spacing d and its dependence on the orientational order, it is particularly interesting to calculate the projection factor $\langle\cos\beta\rangle$ in Eq. (1). Using Eq. (9) with $X=\cos\beta$, we obtained $\langle\cos\beta\rangle=0.83$ for the Sm-A^* and Sm-C^* phases of 8422[2F3], showing that d is about 17% reduced with respect to the rigid-rod length L. With $d=38.7$ Å, taken from the SAXS experiments, we estimated $L=d/\langle\cos\beta\rangle\approx 47$ Å. In the simplest case, L compares to the length of the single extended mesogenic molecule in the smectic phase, but as this length in the present case is only $l=39.4$ Å (cf. Fig. 2), our $L=47$ Å strongly suggests that the smectic layers in this compound are instead built up of aggregates of more than one molecule. Rieker and Janulis [19,20] have studied semifluorinated liquid crystals which in many respects resemble 8422[2F3] and presented experimental evidence that the molecules form aggregates such that the fluorinated chain of one molecule pairs with the nonfluorinated one of its neighbor. Such an aggregate will for the case of 8422[2F3] have a length in the range 47–48 Å (cf. Fig. 2), the exact value depending on the details of the aggregate geometry, fitting very well with our experimentally determined value of L. If and how this strong pair correlation contributes to the absence of smectic layer shrinkage was not conclusively clarified. We will return to this point when we discuss the interlayer correlations in Sec. III D.

To conclude this section, let us summarize the three basic results following from the WAXS experiments.

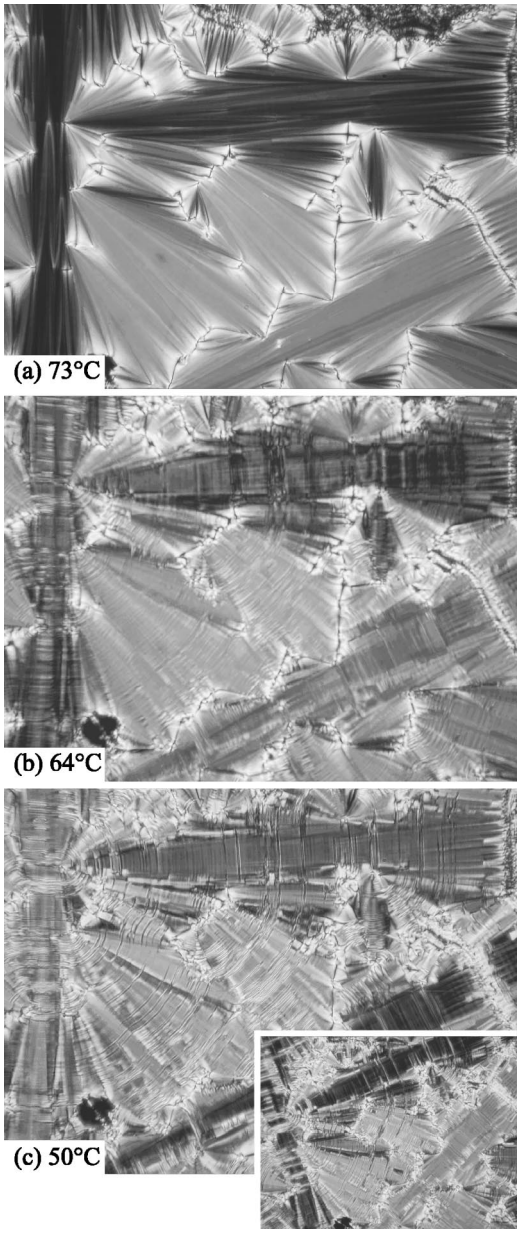

FIG. 7. Textures at 8.5 μm cell gap during a cooling sequence from Sm A^*: (a) Sm A^*, (b) Sm C^* just below the phase transition, (c) Sm-C^*. In the main images, the sample is aligned with respect to the polarizers such that the vertical domain along the left image border is black in the Sm-A^* phase, i.e., in this domain the layers are (on the average) horizontal. In the inset of (c), the sample has been rotated to the new extinction orientation of this domain, 19.5° from the initial orientation.

Compared to ordinary Sm-A and Sm-A^* phases, the Sm-A^* phase of 8422[2F3] exhibits unusually low orientational order. In the rigid-rod approximation, the molecules are, on average, inclined by about 30° with respect to the smectic layer normal.

The orientational distribution found in the Sm-A^* phase remains basically unchanged during the transition to helical Sm-C^* phase. Since there is actually no further increase in the molecular inclination observed, the transition to Sm-C^* phase is of the de Vries type.

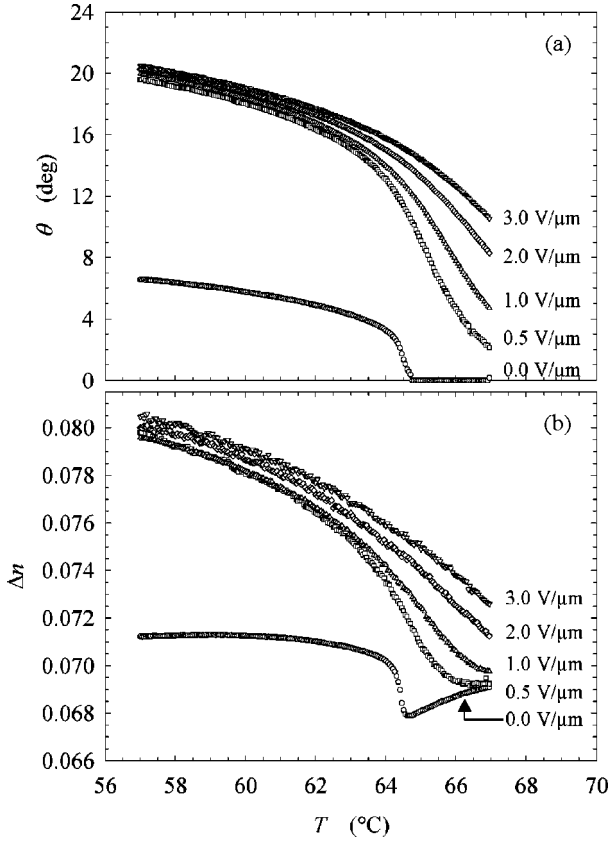

FIG. 8. Optical tilt angle θ (a) and birefringence Δn (b), as a function of temperature T, measured in a 2 μm sample in the virgin surface-stabilized state (0.0 V/μm) and for four different amplitudes of an electric field applied to the sample.

The structural unit that builds up the smectic layers is probably an aggregate of two antiparallel 8422[2F3] molecules.

C. The birefringence and optical tilt

An investigation of the sample texture as a function of temperature and cell gap gave clear evidence of several unique properties of the studied compound. In Fig. 7, the texture at 8.5 μm cell gap during cooling from the Sm-A^* phase is shown. The Sm-A^* texture, Fig. 7(a), had a first-order pink birefringence color. Directly after the phase transition, Fig. 7(b), a quasiperiodic modulation along the layer normal appeared, revealing that the liquid crystal tried to adopt a helical structure. While the helix developed fairly well in some areas, others were clearly nonhelical, i.e., in these areas the sample was surface-stabilized. On further cooling, the helix was expelled in more and more regions, leaving only a few domains with the optic axis along $\hat{z}$ in the texture at 50 °C (c).

A most interesting observation was that the color of the helical regions was very similar to that of the Sm-A^* texture, in contrast to the surface-stabilized regions which were first dark blue close to the transition, then turned cyan at lower temperatures. In other words, the birefringence Δn of the helical Sm-C^* state was approximately the same as in

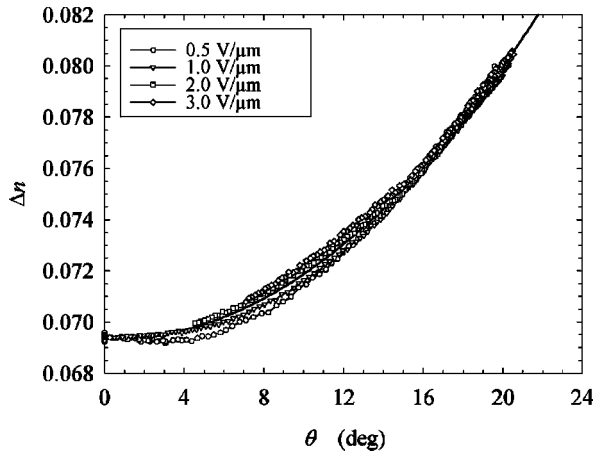

FIG. 9. Birefringence Δn as a function of tilt θ, plotted for several different values of the applied field. All curves essentially fall on a universal functional line, a behavior which is expected from a diffuse cone model A^*-C^* material [16].

Sm-A^* while that of the uniform one was considerably higher. This is quite different from what one expects to see at a Sm-A^*–Sm-C^* transition, in which case the spacial averaging of the optical properties, resulting from the helix formation, radically decreases Δn in the helical state (see, e.g., Ref. [25]). In the surface-stabilized state, one may expect a very small increase of Δn also in regular Sm-C^* materials, due to the transition from a uniaxial to a biaxial state, but the magnitude of this change is far too small to explain the observed color change, see, e.g., Refs. [26,27]. On the other hand, the observed behavior fits very well with the de Vries type Sm-A^*–Sm-C^* transition. As this is a transition from random to ordered molecular tilt, an increased effective Δn must be expected as the optical tilt increases from zero in nonhelical Sm-C^* samples. But if the helix develops, the periodic modulation in φ has the same averaging effect as the Sm-A^* random tilt direction order (assuming a helical pitch as in the present case, i.e., $p \sim 0.5$ μm), leading to identical birefringence and optic axis direction as in this phase.

Using the temperature scanning technique described in Sec. II, these observations could be verified on a quantitative level, as visualized in Fig. 8 for a 2 μm sample. The second-order nature of the Sm-A^*–Sm-C^* transition is clearly seen in both diagrams, displaying the temperature and field dependence of Δn and θ, respectively. Neither in the field-free measurement data nor in those taken while switching the sample is there any sign of discontinuity in any of the observables. It is obvious that the voltage needed for complete switching is very low—even the 1 V θ curve comes very close to the saturated value of θ below the phase transition. At temperatures above the transition, the induced tilt angles are also quite high already at moderate voltages, illustrating the prominent electroclinic effect.

The birefringence measured in the fully switched sample at 57 °C, i.e., in the Sm-C^* phase close to saturation of θ, is 14% larger than that of the relaxed Sm-A^* phase, corroborating the qualitative conclusions based on the 8.5 μm sample textures. The much lower Sm-C^* value of Δn measured in the absence of field signifies that the virgin surface-stabilized structure at low cell gap exhibits inhomogeneities on a scale smaller than the optical resolution, resulting in a certain averaging of the ordinary and extraordinary refractive indices (we will return to the discussion of this state in the following section). Even so, it is still clearly larger than in the Sm-A^* phase. The pronounced minimum in Δn observed at the phase transition is probably connected to light scattering produced by the critical fluctuations at the second-order phase transition [29].

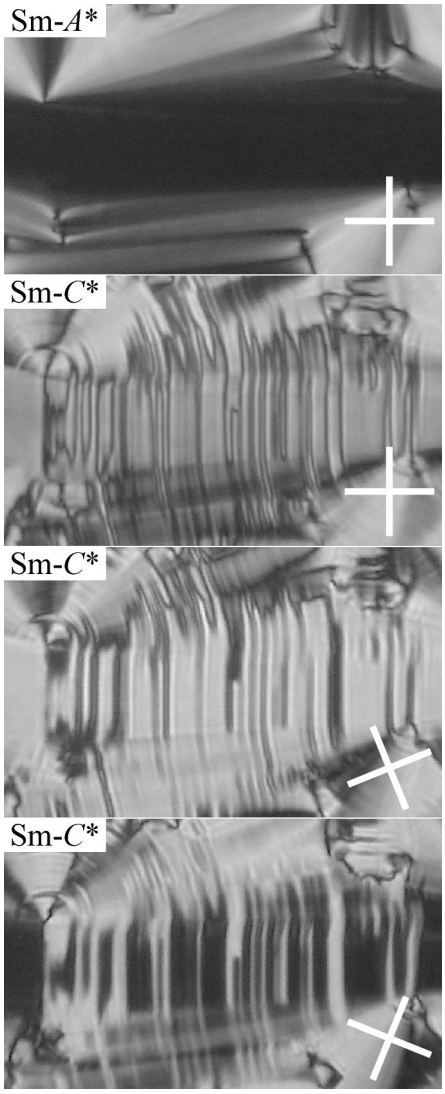

FIG. 10. The peculiar type of ferroelectric domains appearing in the surface-stabilized state of 8422[2F3], observed for the Sm-C^* phase at 5 μm cell gap in the polarizing microscope. The white crosses indicate the orientation of the polarizer cross.

The birefringence is a function of the molecular polarizability and the macroscopic orientational order. As the polarizability can be regarded as constant in the temperature interval investigated, the difference in Δn between Sm-A^* and the switched Sm-C^* state must reflect the difference in orientational order. Using $S_2 = 0.56$ obtained from the x-ray experiments in Sm-A^* phase, the 14% increase in Δn would reflect an ordering to $S_2 = 0.63$. This figure, which should

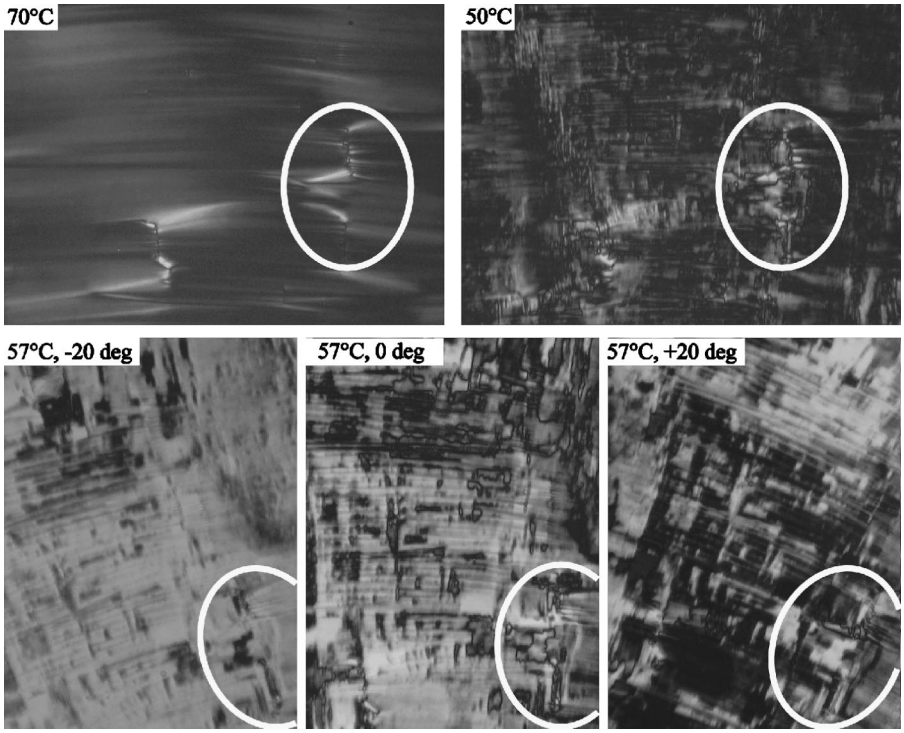

FIG. 11. Textures in the aligned 2 μm EHC cell used for the high-resolution measurements of optical tilt angle and birefringence. The upper row shows the textures of the Sm-A^* phase and of the surface-stabilized Sm-C^* phase before any electric field has been applied, the lower row the textures some 10 min of relaxation after full switching in the Sm-C^* phase at 57 °C. At this temperature the optical tilt angle was measured to be 20°, hence pictures with the smectic layer normal parallel, $+20°$ and $-20°$ to the polarizer cross, are shown. As a guide for the eye, the same characteristic defect has been encircled in all photos.

only be regarded as a rough estimate since the uniaxial order parameter S_2 is not a valid order parameter for the biaxial Sm-C^* phase in the switched state, indicates that even when an electric field strong enough to saturate the electro-optic response is applied, the orientational order is unusually low in 8422[2F3]. The disorder is of course also reflected in the corresponding value of the optical tilt, $\theta = 21°$, which is substantially lower than the average molecular inclination angle $\langle\beta\rangle = 31°$, as determined by the WAXS experiments.

A final evidence that the A^*-C^* transition of 8422[2F3] follows the scheme proposed by de Vries is given in Fig. 9, where Δn is plotted as a function of θ. Selinger *et al.* [16] have developed a theoretical model for the optical properties of a diffuse cone model Sm-A^* phase. One of the predictions of this model is that changes in Δn observed within the Sm-A^* or Sm-C^* phases of the de Vries type, are a function of the optical tilt angle only. This behavior is indeed seen in Fig. 9, where different data sets, corresponding to different values of the applied electric field, fall on the same curve, in agreement with the model.

D. The strength of the interlayer tilt direction correlation

The many peculiar characteristics of the Sm-C^* textures formed by 8422[2F3] actually constitute unusually clear evidence of an extremely weak interlayer tilt direction correlation in this compound. The occurrence of surface stabilization at cell gaps as large as 8 μm would seem to indicate that the helical pitch of the compound is very long. In fact, even at the thickest part of the wedge cell, at 13 μm cell gap, the helix did not form unobstructed. However, as mentioned in Sec. III B 2, we could during the x-ray experiments repeatedly see selective reflection from the sample in the capillary tube, an observation which suggests a pitch in the range of ~ 0.5 μm. Generally, such short-pitch FLC materials develop a uniform helical structure at these cell gaps. But if the correlation in φ across the layer boundaries is very weak, the energy cost of adopting the in-layer twist mediating a helical bulk with an unwound surface structure may be larger than the cost of breaking the chiral interactions producing the helix, thus rendering the surface-stabilized FLC (SSFLC) state favorable at much larger cell gaps than usually expected.

An even more striking evidence is found in studying the shapes of the domains in the SSFLC state, cf. Fig. 10. In contrast to the usual SSFLC domain types, which have approximately equal size along and across the layers, many of the domains in 8422[2F3] have a very small area with an in-layer extension considerably larger than that across the layers. This gives rise to a very large amount of boundaries between domains, which at first seems surprising, as boundaries always cost energy. However, almost all boundaries run along the layers and will therefore, in the case of weak interlayer φ correlation, cost much less energy than the boundaries occurring within layers. Hence, the equilibrium area of the domains is in 8422[2F3] much smaller than in usual FLC materials, and the domain structure has a striking layered character.

The reason for the weak interlayer correlation in φ may well be found in the two-molecule aggregate making up the building-block of the layers, cf. Sec. III B 2. As seen in Fig. 2, both ends of the aggregate end with fluorine atoms. This means that the contact between molecules in adjacent layers is mediated via fluorine-fluorine interactions only, while in most liquid crystals these interactions are mediated via hydrogen atoms. This probably leads to weaker induction and dispersion forces interacting between two adjacent smectic

layers and may thus explain the unusually weak interlayer correlations observed in 8422[2F3].

The texture which was the most difficult to understand was that of the virgin surface-stabilized state which seems to depend very much on the alignment conditions. In some cases twisted states were clearly observed but in the samples discussed here a good extinction and an optic axis inclined with respect to the layer normal was found. Examples of the aligned textures of the 2 μm cell used for the Δn and θ measurements are given in Fig. 11, where the upper row shows the virgin textures and the lower row the relaxed textures after switching with an electric field. At this cell gap the Sm-C^* helix was completely expelled, but the domain texture which spontaneously developed below the A^*-C^* transition temperature was a very unusual one. Rather than the typical SSFLC texture with large up and down domains [28], a ''rippled'' texture, suggesting irregularities on a very small scale, formed. Comparing the Sm-A^* and Sm-C^* textures in the upper row of Fig. 11, it is clear that, in general, the extinction directions only shifted marginally on cooling past the phase transition. The field-free measurements of Δn and θ, shown in Fig. 8, also showed that the effective optic axis only exhibited a small tilt with respect to the layer normal and that the birefringence was much lower than in the uniform switched state.

We believe that the origin of these peculiar properties is a surface-stabilized Sm-C^* state with extremely low correlation length along the layer normal. When the Sm-C^* phase forms in the 2 μm sample, the surface action—which compared to the weak interlayer interactions must be regarded as a very strong external force in cells this thin—completely prevents the formation of the helix. Instead, SSFLC domains are immediately formed directly from a Sm-A^* phase where the molecules are tilted with the same angle as in the Sm-C^* phase but with all values of φ equally probable. As interlayer correlations are very weak, every single layer will, in principle, independently of its neighbors, choose the SSFLC domain type, $+\theta$ or $-\theta$, which is closest to the tilt direction prevailing in the Sm-A^* phase just before the transition. The result will be a virgin SSFLC state exhibiting spatial variations in optical tilt direction on a scale smaller than, or at the limit of, visible light, not too different from the case of an anticlinic Sm-C_a (or Sm-C_a^*) liquid crystal. As the domains are still larger than the regions of uniform orientation in the Sm-A^* phase, a slight increase in birefringence and a small effective tilt angle will be observed.

This state was only seen in the virgin Sm-C^* state at low cell gaps. After the sample had been switched to a uniform alignment, a process which requires a very low voltage, it relaxed to the SSFLC texture shown in the lower row of Fig. 11. The relaxation was extremely slow, which is not surprising as the interlayer interactions are so weak, but after some 10 min a fairly normal SSFLC texture, where macroscopic up and down domains could easily be distinguished, developed. Also in this texture, however, the tendency to form domain boundaries along, rather than across, the layers is obvious, and many areas have a characteristic striped character.

E. The mechanism behind the Sm A^* tilt direction randomization

An important question arising when discussing the de Vries type A-C transition is how the randomization in φ in the Sm-$A(A^*)$ phase is actually produced. Initially, de Vries suggested that the underlying mechanism was a decoupling of the interlayer correlations in φ [14]. This model (in the following referred to as the noncorrelation model) is actually today sometimes [18,30] the one connected to de Vries, despite the fact that in all his later papers he had abandoned this explanation and instead based his reasoning on the much less artificial diffuse cone model. Here, the Sm-A phase does not exhibit a stationary tilt which must be spatially averaged through a random stacking of uniform layers, but the tilt is simply a result of the nematic order fluctuations.

Within the noncorrelation model, it is difficult to explain the properties of the electroclinic effect, not known at the time when the model was first proposed by de Vries, in a chiral de Vries type Sm-A^* liquid crystal. Yet, observation of such a phase, denoted ''Sm-C_R'' (R, random) has been claimed [18]. If each layer is uniformly tilted, and the randomization is strictly related to low correlation across the layer boundaries, each layer must exhibit virtually the same local spontaneous polarization P_s as in the Sm-C^* phase. By applying only a weak electric field (without interlayer correlations there is no obvious strong restoring force, in contrast to helical Sm C^*, where the helix has to be unwound, or the antiferroelectric Sm C_a^*, where the antiferroelectric state has to be broken) the tilt directions therefore ought to be organized on a macroscopic scale. The necessary field strength, and the resulting optical effect, should be in principle independent of the temperature in the Sm-A^* phase. But this is in complete conflict with the strong temperature dependence always observed for the electroclinic effect.

We thus conclude that the main mechanism behind the de Vries type A-C transition cannot be a change in strength in interlayer tilt direction correlation, but rather a biasing of the nematic order fluctuations. An important consequence of this result is that we have a distribution not only in tilt directions φ, but also in tilt magnitudes, β. In all models developed [16] or used [17,18] recently for explaining the macroscopic properties of chiral de Vries type NLS compounds, the randomization is supposed to occur only through fluctuations in φ, while β has a more or less fixed value throughout the Sm-A^* and Sm-C^* phases. This oversimplification may be the reason for the inability of the models to quantitatively describe the optical properties of the investigated compounds.

IV. CONCLUSIONS

The non-layer-shrinkage ferroelectric liquid crystal 8422[2F3] was found to exhibit a second-order ''diffuse cone model'' Sm-A^*–Sm-C^* transition. The nematic orientational order parameter exhibited the same, rather low, value $S_2 = 0.56$ in Sm A^* and helical Sm-C^*, corresponding to an average molecular tilt angle $\langle\beta\rangle = 31°$ in both phases. The layer spacing predicted at such low orientational order com-

pares to the measured values only if a pairwise aggregation of the liquid crystal molecules is assumed. Such aggregation restricts the interlayer molecular interactions to fluorine-fluorine contacts resulting in weak interlayer orientational correlation which was observed experimentally by a very easily disturbed Sm-C^* helix and a peculiar SSFLC texture with domain boundaries running preferentially along the smectic layer interfaces. In the Sm-C^* phase, the azimuthal fluctuations ar biased, leading to a macroscopically observable tilt angle saturating slightly above $\theta = 20°$ at low temperatures. The azimuthal biasing also leads to an increase in effective birefringence on cooling from SmA^* to SmC^* which was found to be close to 15%.

ACKNOWLEDGMENTS

Financial support from the ''German Academic Exchange Service'' (DAAD), from the ''Swedish Foundation for Strategic Research'' (SSF), and the ''Deutsche Forschungsgemeinschaft'' (DFG, Gi 243/2-4) is gratefully acknowledged. We thank J. Ivens and A. Peschel for their assistance in the DSC and SAXS measurements.

[1] T. R. Taylor, S. L. Arora, and J. L. Fergason, Phys. Rev. Lett. **25**, 722 (1970).
[2] T. P. Rieker, N. A. Clark, G. S. Smith, D. S. Parmar, E. B. Sirota, and C. R. Safinya, Phys. Rev. Lett. **59**, 2658 (1987).
[3] F. Giesselmann, P. Zugenmaier, I. Dierking, S. T. Lagerwall, B. Stebler, M. Kaspar, V. Hamplova, and M. Glogarova, Phys. Rev. E **60**, 598 (1999).
[4] M. D. Radcliffe, M. L. Brostrom, K. A. Epstein, A. G. Rappaport, B. N. Thomas, R. F. Shao, and N. A. Clark, Liq. Cryst. **26**, 789 (1999).
[5] Y. Takanishi, Y. Ouchi, H. Takezoe, A. Fukuda, A. Mochizuki, and M. Nakatsuka, Jpn. J. Appl. Phys., Part 2 **29**, L984 (1990).
[6] S. Diele, P. Brand, and H. Sackmann, Mol. Cryst. Liq. Cryst. **16**, 105 (1972).
[7] R. Bartolino, J. Doucet, and G. Durand, Ann. Phys. (Paris) **3**, 389 (1978).
[8] M. Buivydas, S. T. Lagerwall, I. Dierking, F. Gouda, and A. Mochizuki, Ferroelectrics **212**, 67 (1998).
[9] A. de Vries, Mol. Cryst. Liq. Cryst. **11**, 361 (1970).
[10] Y. Takanishi, Y. Ouchi, H. Takezoe, A. Fukuda, A. Mochizuki, and M. Nakatsuka, Mol. Cryst. Liq. Cryst. **199**, 111 (1991).
[11] A. de Vries, J. Chem. Phys. **71**, 25 (1979).
[12] A. de Vries, A. Ekachai, and N. Spielberg, Mol. Cryst. Liq. Cryst. Lett. **49**, 143 (1979).
[13] A. de Vries, in *Advances in Liquid Crystal Research and Applications*, edited by L. Bata (Pergamon Press, Oxford, 1980).
[14] A. de Vries, Mol. Cryst. Liq. Cryst. Lett. **41**, 27 (1977).
[15] A. J. Leadbetter and E. K. Norris, Mol. Phys. **38**, 669 (1979).
[16] J. V. Selinger, P. J. Collings, and R. Shashidhar, Phys. Rev. E **64**, 061705 (2001).
[17] N. A. Clark, T. Bellini, R. Shao, D. Coleman, S. Bardon, D. R. Link, J. E. Maclennan, X. H. Chen, M. D. Wand, D. M. Walba, P. Rudquist, and S. T. Lagerwall, Liq. Cryst. (to be published).
[18] Y. P. Panarin, V. Panov, O. Kalinovskaya, and J. K. Vij, J. Mater. Chem. **9**, 2967 (1999).
[19] T. P. Rieker and E. P. Janulis, Liq. Cryst. **17**, 681 (1994).
[20] T. P. Rieker and E. P. Janulis, Phys. Rev. E **52**, 2688 (1995).
[21] J. P. F. Lagerwall, D. D. Parghi, D. Krüerke, F. Gouda, and P. Jägemalm, Liq. Cryst. **29**, 163 (2002).
[22] A. Saipa and F. Giesselmann, Liq. Cryst. **29**, 347 (2002).
[23] A. Mochizuki and S. Kobayashi, Mol. Cryst. Liq. Cryst. **243**, 77 (1994).
[24] P. Davidson, D. Petermann, and A. M. Levelut, J. Phys. II **5**, 113 (1995).
[25] M. Skarabot, K. Kocevar, R. Blinc, G. Heppke, and I. Musevic, Phys. Rev. E **59**, R1323 (1999).
[26] T. E. Lockhart, E. Gelerinter, and M. E. Neubert, Phys. Rev. A **25**, 2262 (1982).
[27] T. E. Lockhart, D. W. Allender, E. Gelerinter, and D. L. Johnson, Phys. Rev. A **20**, 1655 (1979).
[28] N. A. Clark and S. T. Lagerwall, Appl. Phys. Lett. **36**, 899 (1980).
[29] G. S. Iannacchione, C. W. Garland, P. M. Johnson, and C. C. Huang, Liq. Cryst. **26**, 51 (1999).
[30] Y. P. Panarin, O. E. Kalinovskaya, J. K. Vij, and J. W. Goodby, Ferroelectrics **245**, 763 (2000).